Volume 8 | Number 5 | May 2016 | Pages 463–554

Metallomics

www.rsc.org/metallomics

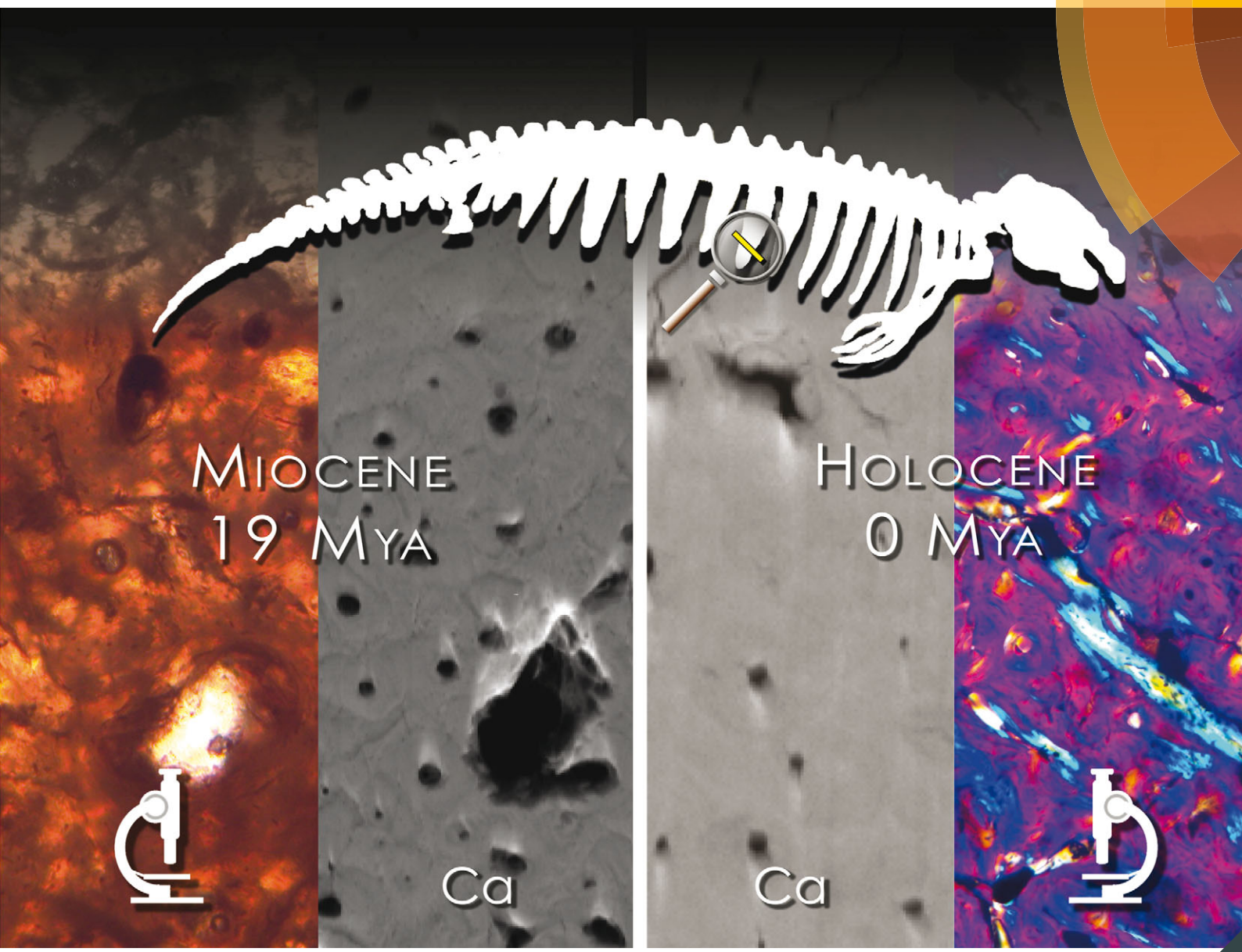

ISSN 1756-5901

ROYAL SOCIETY OF CHEMISTRY

PAPER
Jennifer Anné *et al.*
Chemistry of bone remodelling preserved in extant and fossil Sirenia

Indexed in Medline!

Metallomics

PAPER

Cite this: *Metallomics*, 2016, **8**, 508

Chemistry of bone remodelling preserved in extant and fossil Sirenia†

Jennifer Anné,*[ab] Roy A. Wogelius,[ab] Nicholas P. Edwards,[ab] Arjen van Veelen,[a] Konstantin Ignatyev[c] and Phillip L. Manning[bd]

Received 5th December 2015,
Accepted 24th February 2016

DOI: 10.1039/c5mt00311c

www.rsc.org/metallomics

Bone remodelling is a crucial biological process needed to maintain elemental homeostasis. It is important to understand the trace elemental inventories that govern these processes as malfunctions in bone remodelling can have devastating effects on an organism. In this study, we use a combination of X-ray techniques to map, quantify, and characterise the coordination chemistry of trace elements within the highly remodelled bone tissues of extant and extinct Sirenia (manatees and dugongs). The dense bone structure and unique body chemistry of sirenians represent ideal tissues for studying both high remodelling rates as well as unique fossilisation pathways. Here, elemental maps revealed uncorrelated patterning of Ca and Zn within secondary osteons in both extant and fossil sirenians, as well as elevated Sr within the connecting canals of fossil sirenians. Concentrations of these elements are comparable between extant and fossil material indicating geochemical processing of the fossil bone has been minimal. Zn was found to be bound in the same coordination within the apatite structure in both extant and fossil bone. Accurate quantification of trace elements in extant material was only possible when the organic constituents of the bone were included. The comparable distributions, concentrations, and chemical coordination of these physiologically important trace elements indicate the chemistry of bone remodelling has been preserved for 19 million years. This study signifies the powerful potential of merging histological and chemical techniques in the understanding of physiological processes in both extant and extinct vertebrates.

Introduction

The processes that govern bone physiology utilise a suite of trace elements that can be correlated to specific biosynthetic pathways.[1–3] By mapping and quantifying these trace elements, we can gain a better understanding of these processes and the variation between different tissue types. In addition, the trace elements inventories associated with bone physiology have been shown to preserve in other fossil bone tissues, suggesting the physiology of bone remodelling can be preserved over millions of years.[3] Thus the combination of morphological and chemical preservation allows for a more in depth understanding of the physiology of extinct organisms.

Bone remodelling

The dynamic state of bone results in a high turnover of material through remodelling, allowing the body to cope with changing stresses (shape of bone) and to release essential trace elements held within the apatite structure for use in other biological processes (*e.g.* growth, healing, pregnancy, *etc.*).[4–6] Histologically, remodelled bone can be observed as Haversian systems; a dense network of secondary osteons (a function of the remodelling process) usually observed in older individuals.[4,6] These systems represent a complicated network of osteons and connecting canals (canals connecting osteons) that are heterogenetic in their distribution due to the differential stresses and movement of bone material. Haversian systems are of biological interest as they provide target areas for the study of active bone resorption and deposition.[4–6] If this deposition/resorption cycle is not heavily regulated, it can have a devastating impact on an organism. The pathways and signalling that moderate the cycle of bone deposition and resorption utilise specific trace elements in their regulation including copper, zinc, and strontium.[1–3] Because the degree and distribution of bone deposition/resorption is so varied within the bone tissue, the distributions of these elements can also fluctuate. Thus it is important to look at a larger surface

[a] *University of Manchester, School of Earth, Atmospheric and Environmental Sciences, Williamson Research Centre for Molecular Environmental Science, Manchester M13 9PL, UK. E-mail: jennifer.anne@manchester.ac.uk*
[b] *University of Manchester, Interdisciplinary Centre for Ancient Life, Manchester, M13 9PL, UK*
[c] *Diamond Light Source, Didcot, OX11 0DE, UK*
[d] *Department of Geology and Environmental Geoscience, College of Charleston, 66 George St, Charleston, SC 29424, USA*

† Electronic supplementary information (ESI) available. See DOI: 10.1039/c5mt00311c

This journal is © The Royal Society of Chemistry 2016

area (at the millimetre scale) of both the morphology and chemistry rather than focusing on single histological features (micron).

In the Sirenia (dugongs and manatees) the degree of bone deposition and remodelling is taken to the extreme in a condition known as pachyosteosclerosis, which results in exceedingly dense ribs used for counter buoyancy.[7,8] This unique tissue type makes sirenians an ideal group to study the differential trace element uptake during remodelling as it represents an extreme example of this physiological process. Sirenians also represent a unique aspect of trace element hyperaccumulation as they have been shown to have unique chemical inventories within soft tissues due to a low Cu diet.[9] However, it has not been shown how such trace element inventories are accumulated, maintained and recycled in sirenian bone tissue.[9,10]

Haversian systems and fossilisation

The extremely dense skeleton of Sirenia also present a unique taphonomic condition as the compact bone impedes the diffusion of ground waters compared to the skeleton of other vertebrates. Diffusion models have viewed bone as a homogenous medium, with the only pathway by which groundwater could interact being through surface interactions.[11,12] However, bone tissue is highly variable in both porosity, structure and chemistry, with many micro pores and fractures that increase the pathways and surface area that interact with ground water. In sirenians, the most likely mode of diagenetic alteration is through the complex system of connecting canals within the Havarsian system, which offer one of the few ways for pore water to penetrate into dense bone through the connecting canals between osteons.[13,14] The complexity of the interconnectivity and distribution of these canals can make it difficult to determine the distribution of diagenetic alteration through the use of point analyses.[11–15] Thus the ability to map over larger surface areas allows for the visualisation of such complex chemical pathways that would impact fossilisation, including the vast network of micro pores associated with osteocyte cell networks and Haversian systems.[16] In addition, although there are many diagenetic factors that can alter the chemistry of a fossil, it is possible to differentiate between original organismal (endogenous) chemistry and environmentally mediated (exogenous) material through spectroscopy.

In this study we look at morphological and chemical characterisations of dense bone in extant (*Trichechus manatus*) and extinct (*Metaxytherium* sp.) sirenians to (1) identify the chemical inventories in remodelled bone; (2) see if biomarkers for bone turnover can be preserved in the fossil record; (3) identify the degree and pathway of diagenetic alteration within extremely dense bone tissues.

Methods

Optical histology

Histological sections were used to identify tissue types and to select areas of interest for microfocus mapping. A section of rib from the extant (*T. manatus*; West Indian manatee; NMS.Z 2015.9; Fig. S1, ESI†) and extinct (*Metaxytherium*; PAS11-04; Late Miocene, USA; Fig. S2, ESI†) sirenian ribs were thin sectioned using the petrographic facilities at the School of Earth, Atmospheric and Environmental Sciences (University of Manchester). Thin sections were polished to a thickness of $\sim$50 μm. The thin sections were subject to optical histological analysis using a Nikon petrographic microscope with a camera attachment and viewed under normal and cross-polarised light at 4, 10 and 20× magnification.

Synchrotron analysis

The source billets from the thin sections of extant (*T. manatus*; Fig. S1, ESI†) and fossil (*Metaxytherium*; Fig. S2, ESI†) samples were retained and used for analysis by chemical methods. A complementary set of analyses were obtained for both the extant and fossil specimens *via* synchrotron X-Ray Fluorescence (XRF) elemental mapping, EDS quantification and Extended X-ray Absorption Fine Structure (EXAFS) spectroscopy. No additional sample preparation was performed (embedding, polishing, *etc.*) as such procedures could skew chemical results. Elemental mapping was used to visualise elemental distributions over the various types of histological features identified in optical thin section. Elemental quantification was performed to test whether trace metal concentrations were comparable between the extant and fossil material. EXAFS was used to determine if the local chemical bonding environment of Zn in extant bone was preserved within the fossil.

Specimens were mapped at the microfocus beamline I-18 at the Diamond Light Source (DLS, Oxfordshire, UK), which allows for high resolution (2–10 μm) scans of areas of interest (millimetre scale). This beamline can operate at high incident beam energies (>20 keV), which enables efficient excitation of Sr (E_c = 16.1 keV) and thus allows the mapping and quantification of this critically important component of bone. Specimens were mapped at an incident beam energy of 17 keV (flux 10^{10}–10^{11} photons s^{-1}) using a beam size of 5.5 μm produced *via* Kirkpatrick-Baez focusing mirror. The sample was mounted on an *x*–*y*–*z* translation stage using an SEM carbon tab and raster scanned at a 45° angle to the incident X-ray beam with a four element Si drift Vortex fluorescence detector set at 90° scattering angle.[3,17,18] Mapping, point analyses, and EXAFS at beamline I18 is completed for high atomic weight elements (Ca and higher) in air. Maps were processed using the ROI imaging tool in PyMCA freeware[19] by defining the X-ray emission energy of an element in the recorded EDS spectra.

Quantification was accomplished by taking a full EDS spectrum for 30 seconds at locations of interest revealed through XRF mapping. Three measurements are taken for each location to account for heterogeneity within the bone tissue. EDS spectra were fit using PyMCA, calibrated using a Durango apatite mineral standard, and well-constrained using previous quantification data.[3,17–19] Concentrations obtained using this method were compared with concentrations obtained from PIXE/RBS analysis.

Full Zn K-edge EXAFS were collected for both extant and fossil material to k = 12. The energy of the Zn K-edge was calibrated using a Zn-foil. Background subtraction, data normalization and

fitting of the EXAFS were performed using (d)Athena and (d)Artemis version 0.9.20.[20]

Particle-induced X-ray emission (PIXE)/Rutherford backscattering spectroscopy (RBS)

Conversion of X-ray yield intensity to concentration is complicated by uncertainties regarding matrix composition. Even using the He-purge system, the attenuation of low energy characteristic X-rays from the light elements that dominate organic compounds (especially C, N, O) precludes their analysis at beamline I18. Therefore in order to improve our knowledge of matrix composition and thereby improve the accuracy of our trace element quantification we performed complementary particle beam analysis on the extant sample (*T. manatus*). PIXE and RBS analyses were used to directly measure and map the light element concentrations so that accurate matrix compositions could then be used to refine the XRF results. PIXE/RBS was performed at the Surrey Ion Beam Centre (University of Surrey, Guildford, UK). The setup here allows for both PIXE and RBS data to be taken simultaneously, yielding a combination of fluorescence spectra for elemental quantification and depth profile information which is especially sensitive to proton backscattering from light elements. PIXE/RBS thus allows for the quantification of organic content within the bone, which is not possible using the synchrotron setup at DLS. Due to the high probability of charge build-up with thick sections, thin sections were used instead of the thicker bone billet. The thin section was carbon coated (~10 nm), mounted using double-sided carbon tape, and inserted into the vacuum chamber which contained both an X-ray and particle detector. Specimens were mapped using a 2.5 MeV proton beam (2 MV Tandetron accelerator), with a beam size of 6 × 10 μm. Concentrations were calculated using the raw X-ray and RBS data using a combination of the OMDAQ2007 and GUPIXWIN programs[21] using a Pb glass and Durango apatite standards for calibration of beam parameters. The statistical and fitting error for elemental concentrations was calculated by GUPIXWIN using the peak and background counts for each element.

Results

Fig. 1 shows the similarities in both histology and trace element distributions between the extant (*T. manatus*) and fossil (*Metaxytherium*) samples. Optical light histology shows tissue types consisting mainly of a dense mixture of primary and secondary osteon (white circle). These features are identified by the circular pattern of the lacunae (small space containing an osteocyte), seen in optical histology as small, elongated black dots. In the elemental maps of Ca, a bright (relatively higher concentration)

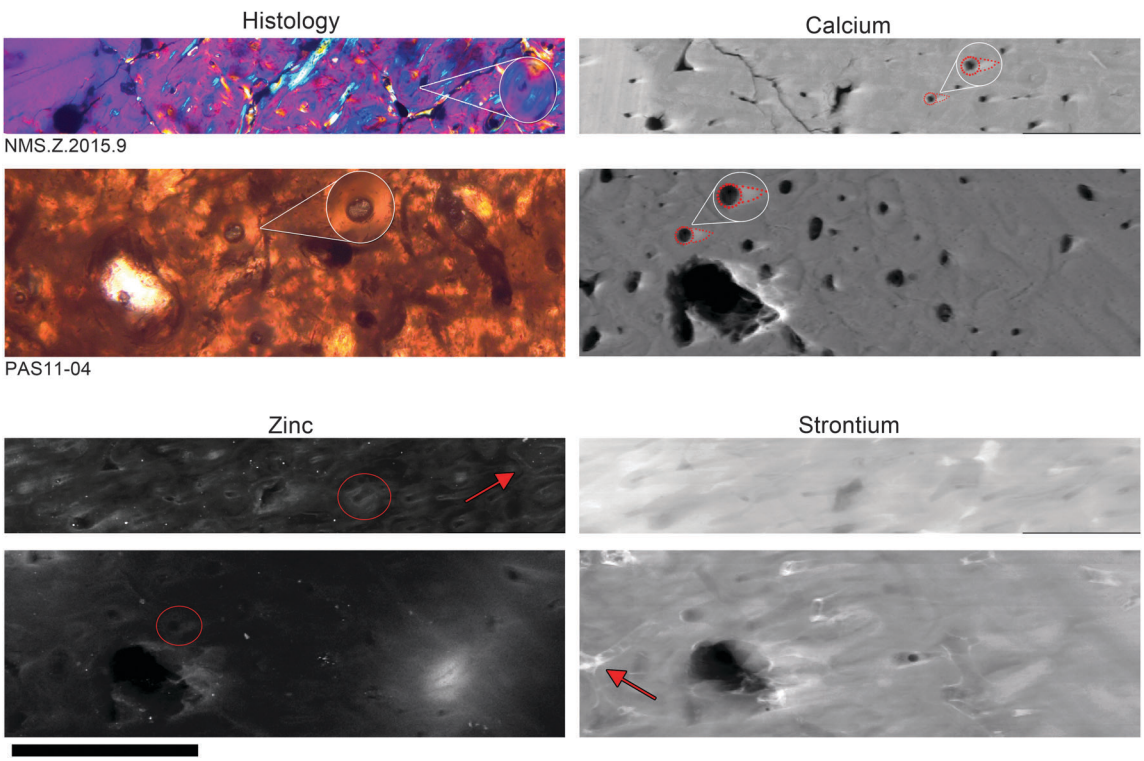

Fig. 1 Optical thin sections of *T. manatus* (NMS.Z 2015.9) and *Metaxytherium* (PAS11-04) compared to microfocus (DLS) elemental maps of Ca, Zn and Sr. Histological views are represented in cross-polarized light (*Metaxytherium*) with a lambda filter (*T. manatus*). Extant and fossil material is comparable in both optical histology and elemental distributions with the exception of Sr. Optical histology shows primary and secondary osteons (examples highlighted in white inserts). The extent of the cutting cones can be observed in Ca as 'comet tails' coming off the opening of the secondary osteon (examples highlighted in white inserts). Zn is concentrated within bone deposited within the secondary osteons (examples circled in red), and along the lining of connecting canals between osteons (red arrow). Sr is relatively evenly distributed throughout the bone tissue in the extant *T. manatus* specimen, but is concentrated within the connecting canals of the fossil specimen (example highlighted with red arrow). Scale is 1 mm.

This journal is © The Royal Society of Chemistry 2016

Table 1 Quantification of trace elements in *T. manatus* using synchrotron and PIXE analyses and *Metaxytherium* using synchrotron analyses. "Osteon" refers to the cylindrical compact bone tissue around the Haversian canal openings. "Bone" refers to all other bone tissues. Concentrations are given in ppm or weight percent (wt%). Conservative 2σ error for all DLS data as well as Ca *via* PIXE are ~10% of the absolute value. Error estimates for PIXE trace metals are given as percent error (%)

	Synchrotron					PIXE	
		T. manatus		*Metaxytherium*			*T. manatus*
Element	Durango standard	Bone	Osteon	Bone	Osteon	Durango standard	Bulk
Ca (%)	38.19	40.34	39.86	31.32	32.31	46.01	42.26
Mn	—	11	18	175	190	—	—
Fe	397	72	117	6317	7217	333(7.7)	94(2.9)
Ni	—	8	9	21	27	—	100(12.2)
Cu	—	11	18	36	44	—	26(10.4)
Zn	27	244	477	161	234	35(35.3)	340(1.7)
As	797	3	3	9	15	839(5.3)	—
Sr	669	1326	1444	3105	3204	982(9.9)	1338(2.2)

'comet tail-like' structure extends from the secondary osteon in both specimens (highlighted insert), indicating the size and shape of the cutting cone. Elemental maps of Zn show elevated concentrations within the infilled bone tissue of the secondary osteons (extant and fossil; red circle) and the lining of the connecting canals (extant; red arrow). The only difference in elemental distributions between extant and fossil material is seen in Sr, which is concentrated within the connecting canals of the fossil (red arrow) and as a wash within extant material.

For extant material (*T. manatus*), the concentrations obtained through synchrotron analysis are consistent with those obtained by PIXE/RBS. The collagen–apatite ratio was calculated at 1 : 3 (~33% collagen) based on RBS profiles (Fig. S3, ESI†). Dismissing the effect of collagen on trace element calculation resulted in large quantification errors, resulting in improbable (potentially toxic) concentrations (Table S1, ESI†). Elemental concentrations were comparable between extant and extinct specimens when collagen was included in the stoichiometry with the exception of highly elevated Mn and Fe in the fossil (Table 1).

EXAFS revealed Zn to be in tetrahedral coordination with four oxygens at 1.95 Å in both extant and fossil samples (Fig. 2; Table 2). This is consistent with Zn substituting into the Ca^2 site, similar to the Zn coordination found in both bio and non-bio Zn-HAP.[22,23] The *k*-space data for each are similar with peaks aligned at 2, 4, 6, 8, and 10 $Å^{-1}$. After Fourier-transforming the data, Fig. 2B shows how the first shell arrangements of atoms around the central Zn absorber is virtually the same in both specimens.

Discussion

Elemental mapping revealed trace elements associated with bone remodelling (Ca and Zn) to be concentrated within discrete histological features of dense Haversian bone in the sirenians, *T. manatus* (NMS.Z 2015.9) and *Metaxytherium* (PAS11-04). Such imaging could only be resolved using the combined sensitivity and resolution of synchrotron-based mapping. Ca distributions are seen as comet tail-like structures interpreted here as the three-dimensional structure of the cutting cone in both extant and fossil samples. An alternative interpretation of these features is a shadow effects caused by beam geometry. However, as these

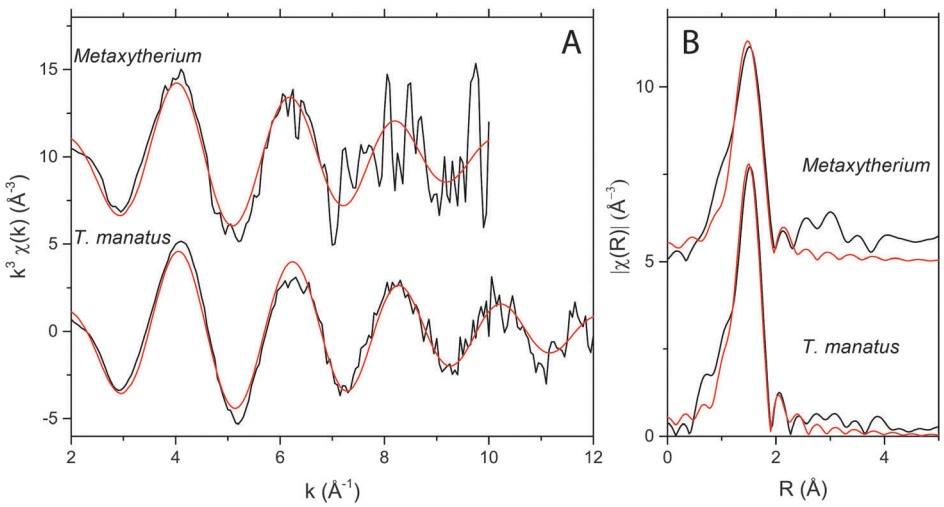

Fig. 2 Zn EXAFS for *Metaxytherium* sp. and *T. manatus* showing EXAFS (A) *k*-space data (black curve) with fit (red curve) along with the (B) Fourier transformed *R*-space results (data = black curve; fit = red curve). The coordination chemistry of Zn in this fossil and in the extant bone is the same.

Table 2 Fit statistics for Zn EXAFS in *T. manatus* and *Metaxytherium* using (d)Artemis. Errors are given as (±) the last significant figure unless specified. Error for CN is 25%

Specimen	Path	CN	R (Å)	σ^2 (Å^2)	ΔE_0 (eV)	$S_0{}^2$	χ^2	R
T. manatus	Zn–O	4.4	1.95(07)	0.007(1)	1.95 ± 0.77	0.99(3)	92	0.01
Metaxytherium	Zn–O	4.4	1.97(04)	0.009(08)	2.32 ± 0.39	1.00(4)	17.82	0.019

features are only present in certain elements and not all, the more likely cause is enrichment by biological processes. Pooling of Ca within the cutting cone can be attributed to osteoblastic regulation of mineralisation during deposition, where osteoblasts membrane-bound matrix vesicles concentrate Ca and P.[24] Elevated Ca could also be caused by an increase of free Ca released from the bone during the resorption stage of remodelling.[4,6]

Elemental maps of Zn revealed higher concentrations within the lining of the connecting canals between osteons (NMS.Z 2015.9) and around secondary osteons within the Haversian system (both). This is similar to findings in previous studies on human osteons as Zn is known to pool in forming osteons, especially within the area of osteoid at the mineralisation front.[1,2,25] The overall elevated concentrations of Zn alludes to the heavy demand for bone-regulating trace elements within remodelled bone, with Zn playing a crucial role in healthy bone development.[26] Elevated levels of Zn also fits with the findings of high Zn in the liver of extant *Dugong dugon*, where Zn was found in concentrations of up to 4 wt%.[9] Concentrations of Zn are comparable between extant and fossil bone, indicating Zn has not been significantly added or lost during fossilisation. Zn EXAFS of the fossil bone is comparable to the coordination seen in the extant manatee (Fig. 2), strongly supporting the conclusion that the Zn in the fossil bone is endogenous and the observed distribution or Zn has been preserved through deep time.

Sr is elevated in both extant and fossil manatee bone samples compared to normal bone concentrations previously determined in the bones of other marine mammals, however the levels found here are within the concentration range measured in extant dugong tusks (1709–2155 ppm).[10,26–28] Elevated levels of Sr in manatee bone may be attributed to two factors. Firstly, Sr concentrations tend to be high for bone grown within from marine environments. Secondly, Sr concentrations tend to be higher in herbivores *versus* carnivores[26] for species from the same environment. Therefore manatees, as marine herbivores, would be expected to have relatively high Sr contents in their bones. Furthermore, high Sr is expected in bone *versus* soft tissue as the biological deposition of Sr is almost exclusively within bone, where it substitutes for Ca in mineralized tissue.[28,29] Sr is also known to concentrate in areas of high rates of remodelling and repair as it is an important element in the regulation of osteoclasts.[25,29] We also note that the connecting canals of PAS11-04 are preferentially enriched in Sr, highlighting the detailed connectivity of the complex Haversian system (Fig. 1). The Sr enrichment at the surfaces of the connecting canals may be due to biological substitutions as discussed above, or it may also reflect post-mortem mass transfer of Sr into the exposed internal canal surfaces from geochemical fluids, because Haversian systems may provide ground water infiltration pathways during diagenesis.[11]

Elemental concentrations calculated for NMS.Z 2015.9 are within the expected range for marine vertebrates.[8,9,25,27] Most importantly, it was found that the inclusion of organic components within the matrix stoichiometry in the fit calculations greatly affected and improved trace element quantification (Fig. S3, ESI†). This was most noticeable in Zn, which was initially highly elevated compared to known biological concentrations from both PIXE and synchrotron analysis when collagen was not included in the experimental parameters (sample matrix stoichiometry; Table S1, ESI†). This affect was not seen in previous analyses of extant material,[3] however, all previous studies have been conducted mainly on avian material, which in museum collections can dry quickly due to the thinness of the bone and low concentrations of marrow. We suggests then that the thickness and density of the sirenian bone may have allowed it to retain more of its organic constituents and we caution future studies that apply chemical techniques to bone that remove or do not take into account organics for matrix stoichiometry.

Conclusion

The combination of detailed morphological and chemical analyses resulted in the imaging of bone remodelling pathways in both extinct and extant Sirenia. Elemental mapping of remodelled bone in *T. manatus* revealed strong correlations between histological features and the elements Ca and Zn. These distributions highlight morphological features and provide evidence for active physiological processes occurring up to the time of death. In particular Zn is found around areas of active ossification. The same trace element distributions are seen in a fossil sirenian, *Metaxytherium*, indicating that original biochemistry has been preserved for ~19 million years. Elemental mapping also reveals complex histological structures such as connecting canals; features that cannot be seen in optical microscopy. Thus the application of synchrotron-based elemental imaging and spectroscopy combined with optical histological analyses can be used to not only strengthen the correlation between morphology and physiological processes, but also help visualise and provide a better understanding of how bone tissue morphology and chemistry can affect fossilisation pathways.

Acknowledgements

We thank Dr Peter Dodson of the University of Pennsylvania, the Surrey Ion Beam Centre and Dr G. Grime (University of Surrey), NERC (NE/J023426/1), STFC, the Jurassic Foundation (awarded J. A.) the University of Manchester Dean's Fund (awarded J. A.), the Diamond Light Source for access to beamline

 This journal is © The Royal Society of Chemistry 2016

I18 (SP8597, SP9488-1), and the reviewers for their insightful comments. Prof. Manning thanks STFC for their continued support at both the Diamond Lightsource and the STFC PE Fellows.

References

1 S. Gomez, R. Rizzo, M. Pozzi-Mucelli, E. Bonucci and F. Vittur, *Bone*, 1999, **25**(1), 33–38.
2 S. Haumont, *J. Histochem. Cytochem.*, 1960, **9**, 141–145.
3 J. Anné, N. P. Edwards, R. A. Wogelius, A. R. Tumarkin-Deratzian, W. I. Sellers, A. van Veelen, U. Bergmann, D. Sokaras, R. Alonso-Mori, K. Ignatyev, V. M. Egerton and P. L. Manning, *J. R. Soc., Interface*, 2014, **11**(96), 20140277.
4 L. G. Raisz, *Clin. Chem.*, 1999, **45**(8B), 1353–1358.
5 R. F. M. van Oers, R. Ruimerman, E. Tanck, P. A. J. Hilbers and R. Huiskes, *Bone*, 2008, **42**, 250–259.
6 N. B. Watts, *Clin. Chem.*, 1999, **45**(8B), 1359–1368.
7 V. Buffrénil, A. Canoville, R. D'Anastasio and D. P. Domning, *J. Mamm. Evol.*, 2010, **17**(2), 101–120.
8 D. P. Domning and V. Buffrénil, *Mar. Mammal Sci.*, 1991, **7**(4), 331–368.
9 G. R. W. Denton, H. Marsh, G. E. Heinsohn and C. Burdon-Jones, *Mar. Biol.*, 1980, **57**(3), 201–219.
10 J. S. Edmonds, Y. Shibata, R. I. T. Prince, A. R. Preen and M. Morita, *Mar. Biol.*, 1997, **129**(2), 203–214.
11 M. J. Kohn, *Geochim. Cosmochim. Acta*, 2008, **72**(15), 3758–3770, DOI: 10.1016/j.gca.2008.05.045.
12 M. J. Schoeninger, K. M. Moore, M. L. Murray and J. D. Kingston, *Appl. Geochem.*, 1989, **4**, 281–292.
13 M. J. Kohn and R. J. Moses, *Proc. Natl. Acad. Sci. U. S. A.*, 2013, **110**(2), 419–424, DOI: 10.1073/pnas.1209513110.
14 M. B. Goodwin, P. G. Grant, G. Bench. and P. A. Holroyd, *Palaeogeogr., Palaeoclimatol., Palaeoecol.*, 2007, **253**(3–4), 458–476, DOI: 10.1016/j.palaeo.2007.06.017.
15 D. Herwartz, T. Tütken, K. P. Jochum and P. M. Sander, *Geochim. Cosmochim. Acta*, 2013, **103**, 161–183, DOI: 10.1016/j.gca.2012.10.038.
16 B. Hesse, P. Varga, M. Langer, A. Pacureanu, S. Schrof, N. Männicke, H. Suhonen, P. Maurer, O. Cloetens, F. Peyrin and K. Raum, *J. Bone Miner. Res.*, 2015, **30**(2), 346–356, DOI: 10.1002/jbmr.2324.
17 V. M. Egerton, R. A. Wogelius, M. A. Norell, N. P. Edwards, W. I. Sellers, U. Bergman, D. Sokras, R. Alonso-Mori, K. Ignatyev, A. van Veelen, J. Anné, B. van Dongen, F. Knoll and P. L. Manning, *J. Anal. At. Spectrom.*, 2015, **30**, 627–634.
18 N. P. Edwards, P. L. Manning, U. Bergmann, P. L. Larson, B. E. van Dongen, W. I. Sellers, S. M. Webb, D. Sokaras, R. Alonso-Mori, K. Ignatyev, H. E. Barden, A. van Veelen, J. Anné, V. M. Egerton and R. A. Wogelius, *Metallomics*, 2014, **6**(4), 774.
19 V. A. Solé, E. Papillon, M. Cotte, P. H. Walter and J. Susini, *Spectrochim. Acta, Part B*, 2007, **62**, 63–68.
20 B. Ravel and M. Newville, *J. Synchrotron Radiat.*, 2005, **12**, 537–541.
21 J. A. Maxwell, W. J. Teesdale and J. L. Campbell, *Nucl. Instrum. Methods Phys. Res., Sect. B*, 1995, **95**(3), 407–421.
22 D. Bazin, X. Carpentier, I. Brocheriou, P. Drofmuller, S. Aubert, C. Chappard, D. Thiaudière, S. Reguer, G. Waychunas, P. Jungers and M. Daudon, *Biochimie*, 2009, **91**, 1294–1300.
23 Y. Tang, H. F. Chappell, M. T. Dove, R. J. Reeder and Y. J. Lee, *Biomaterials*, 2009, **30**(15), 2864–2872.
24 B. Clarke, *Clin. J. Am. Soc. Nephrol.*, 2008, **3**(suppl. 3), S131–S139.
25 B. Pemmer, A. Roschger, A. Wastl, J. G. Hofstaetter, P. Wobrauschek, R. Simon, H. W. Thaler, P. Roschger, K. Klaushofer and C. Streli, *Bone*, 2013, **57**, 184–193.
26 R. Eisler, *Compendium of Trace Metals and Marine Biota*, Elsevier Science, Oxford, UK., 2009.
27 J. C. Sealy and A. Sillen, *J. Archaeol. Sci.*, 1988, **15**, 425–438.
28 Y. Fujise, K. Honda, R. Tatsukawa and S. Mishima, *Mar. Pollut. Bull.*, 1988, **19**(5), 226–230.
29 T. Swanston, T. Varney, I. Coulthard, R. Feng, B. Brewer, R. Murphy, C. Hennig and D. Cooper, *J. Archaeol. Sci.*, 2012, **39**(7), 2409–2413, DOI: 10.1016/j.jas.2012.01.041.